Korean Journal of Chemical Engineering (2024) 41:2717–2727
https://doi.org/10.1007/s11814-024-00178-2

ORIGINAL ARTICLE

Leaching Behavior of the Main Metals of Decopperized Anode Slime

Xun Zhou[1] · Chunfa Liao[1] · Fupeng Liu[1] · Yanliang Zeng[1]

Received: 17 February 2024 / Revised: 10 April 2024 / Accepted: 22 April 2024 / Published online: 27 April 2024

Abstract
Clarifying the occurrence state and embedding characteristics is the primary task to investigate the leaching behavior of the main metals in decopperized anode slime. Electron probe microanalysis, thermodynamic analysis, and leaching experiments were used to determine the optimum conditions for efficient one-step separation of the scattered and precious metals (SPMs) from base metals. The result shows that the leaching efficiencies of Te, Au, Pt, and Pd were 97.69%, 100.79%, 94.47%, and 100.38%, respectively. Moreover, there was scarcely leaching of Pb, Sn, Sb, and Ag, with most of Bi and As remaining in the residue. Te, Au, Pt, and Pd enriched in a targeted manner. This work presents that it is useful in the analysis of the phenomena in copper anode slime hydrometallurgy and provides a short process technology for treating the decopperized anode slime.

Keywords Copper anode slime · Scattered and precious metals · Chloridizing leaching · Leaching behavior

Introduction

According to the World Copper Factbook 2023, the world's refined copper production reached 25.7 million tons in 2022, of which 80.4% was through copper electrolytic refining routes [1]. Copper anode slime is an inescapable by-product produced during the copper electrolytic refining process, accounting for approximately 0.2–0.8% of refined copper production [2]. Copper anode slime contains scattered and precious metals (SPMs) such as Au, Ag, Pt, Pd, Se, Te, and various base metals such as Pb, As, Sb, Bi, Sn, Cu, etc. [3, 4]. SPMs are not only critical materials for modern industry, national defense, and strategic emerging industries but also indispensable resources for national socioeconomic development and national defense construction [5–9]. In China, over 40% of Au, Ag, Se, and Te come from copper anode slime [10]. Globally, the demand for SPMs is growing faster than the demand for other metals [11].

Recently, various technologies have been developed to separate SPMs from base metals in copper anode slime. Liu [2] gradually separated base metals such as Cu, Ni, As, Pb, and Sn, with Ag and Au enriched in the residue. Khanlarian [12] achieved efficient and low-consumption leaching of Se, Cu, and Ag using a low-temperature mineral phase reconstruction method. In addition, research on wet craftsmanship, such as oxide acid immersion [13], oxygenic acid immersion [14], and mineral selection [15], is increasingly prosperous. Wet chlorination enables the formation of soluble base metal components (like As, Sb, and Bi) chlorides in copper anode slime, which are detrimental to copper ore [16]. As in the process of tellurium extraction, the impurity influencing factors are Se > Sb > As > Cu [17]. Meanwhile, in the extraction of Au from chlorine solution, Pb^{2+} will deteriorate the reduction efficiency of Au [18]. In summary, major existing SPMs processes aim to recycle a single metal. Generally, problems such as uneven metal types, low leaching efficiency, or narrow application range of raw materials are the limitations, as difficulty lies in the significant interference of base metals such as, Sb, and Bi on the separation and extraction of SPMs.

Our previous studies [10, 19] have clarified the selective separation and precipitation behavior of As, Sb, and Bi and revealed the selective separation and volatilization kinetics mechanism of Se. Regrettably, the occurrence and leaching behavior of base metals (such as Pb and Sn) and platinum group metals (Pt and Pd) was not studied. Herein, the objective of this study is to systematically investigate the leaching behavior of the main elements, achieve targeted enrichment of the Au, Te, Pt, and Pd, and form a short process technology for efficient separation of the SPMs from copper anode slime.

✉ Chunfa Liao
liaochfa@163.com

[1] School of Metallurgical Engineering, Jiangxi University of Science and Technology, Ganzhou 341000, China

Table 1 Particle size analysis parameters and the results of the decopperized anode slime

Analysis	Particle refractive index	Dispersant refractive index	Scattering model	Analysis model	Weighted residual	Laser opacity
	1.730	1.330	Mie	General	0.41%	10.12%
Result	Span	Consistence	Specific surface area	D_{10}	D_{50}	D_{90}
	2.631	0.834	2109 m^2/kg	1.038 μm	5.636 μm	15.868 μm

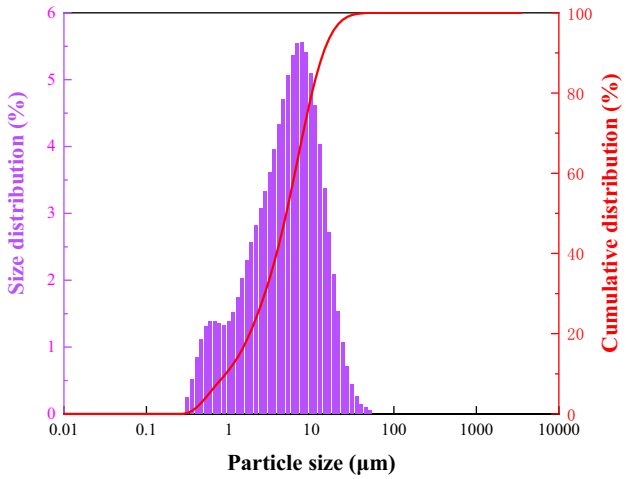

Fig. 1 Particle size distribution curve of the decopperized anode slime

Experimental

Experimental Materials

The experimental raw material is the decopperized anode slime from a copper smelting enterprise in southern China. This enterprise includes directional removal of As, Sb, and Bi by composite acid leaching, recovery of Se by sulfuric acid roasting, and separation of Cu by washing the roasted slag with water. The washed residue is the decopperized anode slime. Particle size analysis of the decopperized anode slime was performed using a laser particle size analyzer (Mastersizer3000). The parameters and results of the laser particle size analysis are presented in Table 1, and the particle size distribution curve is shown in Fig. 1. The particle size of 100% of the decopperized anode slime is below 74 μm. The particle size distribution curve shows a normal distribution, which is favorable for the sampling uniformity.

The chemical compositions of the decopperized anode slime are presented in Table 2. The copper anode slime contains 8.91% Ag, 0.60% Au, 4.81% Te, 45.05 g/t Pt and 182.85 g/t Pd, whereas the Ba, Pb, Sn, Sb, As, Bi, Cu, and Se contents are 22.14%, 18.93%, 7.18%, 2.03%, 0.54%, 0.41%, and 0.09%, respectively, indicating that this decopperized anode slime has an urgent recovery value. From the X-ray diffraction pattern of the raw materials, several diffraction peaks are related to SnO_2, AgCl, $BaSO_4$, $(Ba_{0.69}Pb_{0.31})SO_4$, and TeO_2, as shown in Fig. 2. Because of the low content of Sb, Au, Pd, and so on, no diffraction peaks of each phase were observed.

Figure 3 illustrates the distribution maps of the main elements present in the raw materials. There are irregular large particles, rod-shaped particles, amorphous flocculent small particles, and bright spots, as shown in Fig. 3. Based on the distribution of elements, irregular large particles consist of a core layer and a shell layer, in which the shell layer was (Ba, Pb)SO_4 and the core phase was $BaSO_4$. The rod-shaped particles are tin oxide. Silver was distributed in flocculent small particles, with a small portion embedded in irregular large particles. Arsenic coexisted with Ag and O. Antimony was present in addition to Ag with O and can also be present together with Sn. Bismuth was present with the (Ba, Pb)SO_4 shell layer. The occurrence of partial tellurium is like that of Sb and partial tellurium had a highly overlapping distribution of Ag and Au, respectively. This indicates that tellurium oxide, silver telluride, and gold telluride were presented in the raw materials. Copper was embedded in tin oxide. There was no enrichment of selenium or platinum. Bright spots consisted of Au and Pd. To determine the exact composition

Table 2 Main chemical components of the decopperized anode slime

Element	Ba	Pb	Ag	Sn	Te	Sb	Au
Content (wt%)	22.14	18.93	8.91	7.18	4.81	2.03	0.60
Element	Cu	As	Bi	Se	Pt	Pd	
Content (wt%)	0.39	0.54	0.41	0.09	45.05 g/t	182.85 g/t	

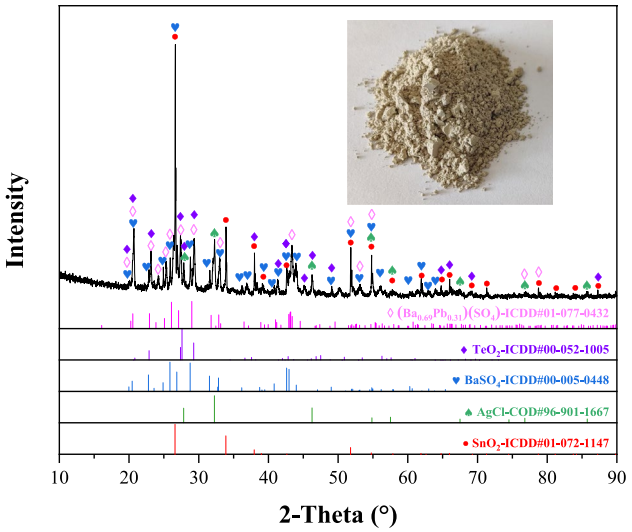

Fig. 2 X-ray diffraction pattern of the decopperized anode slime

of the decopperized anode slime, several points (as shown in Fig. 4) were selected for quantitative analysis using EPMA. Table 3 presents the results.

According to the quantitative data in Table 3 and the distribution of elements in Fig. 3, the point 1 particle was identified as Ag_2Te, AgCl, Ag_2SO_4, TeO_2, Te, $(Ba_xPb_y)SO_4$, SnO_2, CuO, and a few As_2O_3, Bi_2O_3, Pt, or PtO_2. The floc at point 2 was identified as AgCl, Ag_2SO_4, TeO_2, $(Ba_xPb_y)SO_4$, SnO_2, CuO, As_2O_3, Bi_2O_3, Pt, or PtO_2. The bright spot at point 3 was identified as Au, Pt, Pd, and Ag. The presence of $(Ba_xPb_y)SO_4$ is due to the selection area encompassing a small portion of the dark matrix, as shown in Fig. 4a. The fine particle in point 4 was mainly composed of AgCl, Ag_2SO_4, Ag_2O, TeO_2, SnO_2, CuO, and a small amount of As_2O_3, Bi_2O_3, Au, and Pt. Point 5 particle mainly contained $(Ba_xPb_y)SO_4$, AgCl, TeO_2, Ag_2SO_4, and a few Au. Point 6 was identified as SnO_2. In addition to Cu, SnO_2, Cu_2Te, and Sn, there were also small amounts of $(Ba_xPb_y)SO_4$, Ag_2Te, AgCl, and Bi_2O_3 in the blocky particles of point 7. Point 8 particle comprised AgCl, TeO_2, Sb_2O_3, Ag_2O, $CuSO_4$, $(Ba_xPb_y)SO_4$, and small amounts of As_2O_3, Bi_2O_3, Pt, Pd, or PtO_2 and PdO. It was indicated that part of the Ag was wrapped in $BaSO_4$ core phase and that a small amount of Sb_2O_3, CuO, As_2O_3, Bi_2O_3, Pt, Pd, Ag, and Ag_2Te were mixed in the $(Ba_xPb_y)SO_4$ shell phase from points 9 and 10. Point 11 particle was composed of AgCl, Ag_2Te, Ag_2SO_4, Sn, SnO_2, TeO_2, $(Ba_xPb_y)SO_4$, and small amounts of CuO, As_2O_3, Bi_2O_3, and PtO_2. Point 12 was mainly composed of Au, AgCl, $(Ba_xPb_y)SO_4$, $AuTe_2$, Ag_2SO_4, and a small amount of Cu, SeO_2, Pt, Pd, As_2O_3, and Bi_2O_3. Compared with points 3 and 12, point 13 can better explain the enrichment phenomenon of SPMs, which mainly consisted of Au, Pd, and Ag_2Se. The occurrence state and embedding characteristics of the main metal element in the decopperized anode slime are summarized in Table 4. To verify the EPMA analysis result, chemical analysis was used to identify the mineral phases of Cu, Ag, and Te in the decopperized anode slime, as shown in Table 5.

Summarily, tellurium was identified as five occurrence states: Ag_2Te, TeO_2, Te, $AuTe_2$, and Cu_2Te. In addition to Ag_2Te, silver also was identified as AgCl, Ag_2SO_4, Ag_2O, Ag, and Ag_2Se. Gold was identified as two types of objects: Au and $AuTe_2$. Most platinum and palladium were present in the metallic phase, but there may still be a small amount of their oxides coexisting with Ag-enrichment. Interestingly, most SPMs, such as Te, Au, Pt, and Pd were distributed in active regions, such as the surface of particles with a large specific surface area and alloy phase. On the contrary, base metals, such as Pb, Ba, and Sn, were distributed in stable particles, such as sulfate blocks and rod-shaped particles.

Experimental Principle and Method

According to the phase analysis results, Table 6 lists the possible reactions of the existing phases during chlorination leaching. The Gibbs free energy changes of reactions (1)–(17) were calculated using the Reaction module in Factsage 8.1 [20] and plotted as a $\Delta G_r^{\theta}-T$ diagram, as shown in Fig. 5. Thermodynamic data are obtained from the FactPS database and the aqueous solutions [21, 22]. As shown in Fig. 5, the ΔG_r^{θ} of reactions (1)–(17) are all negative, indicating that the SPMs phases will undergo reactions during the chlorination leaching process. Furthermore, tellurium, gold, platinum, and palladium will present in the solution in the form of $TeCl_6^{2-}$, $AuCl_4^-$, $PtCl_6^{2-}$, and $PdCl_4^{2-}$, respectively, while silver will exist in the residue in the form of AgCl.

The specified concentration of the mixture of H_2SO_4 and NaCl was added to the beaker, a certain mass of the decopperized anode slime and $NaClO_3$ were added and stirred well, then transferred to a heating magnetic stirrer (DF-101S) and set to a temperature ranging from 5 °C to 95 °C, with stirring at 350 rpm. During leaching, the beaker was sealed with plastic wrap to reduce the evaporation of the solution.

Analytical Method

The main phases were identified by X-ray diffraction (XRD, PANalytical X'Pert Pro Powder, Almelo, the Netherlands) using a CuKα radiation source with an acceleration potential of 40 kV and a current of 40 mA. XRD diffractograms were analyzed using HighScore Plus software. The concentrations of Pb, Sn, Ag, Sb, Se, Cu, Bi, Te, Au, Pt, and Pd were determined by inductively coupled plasma optical emission spectroscopy (ICP-AES, Thermo Electron

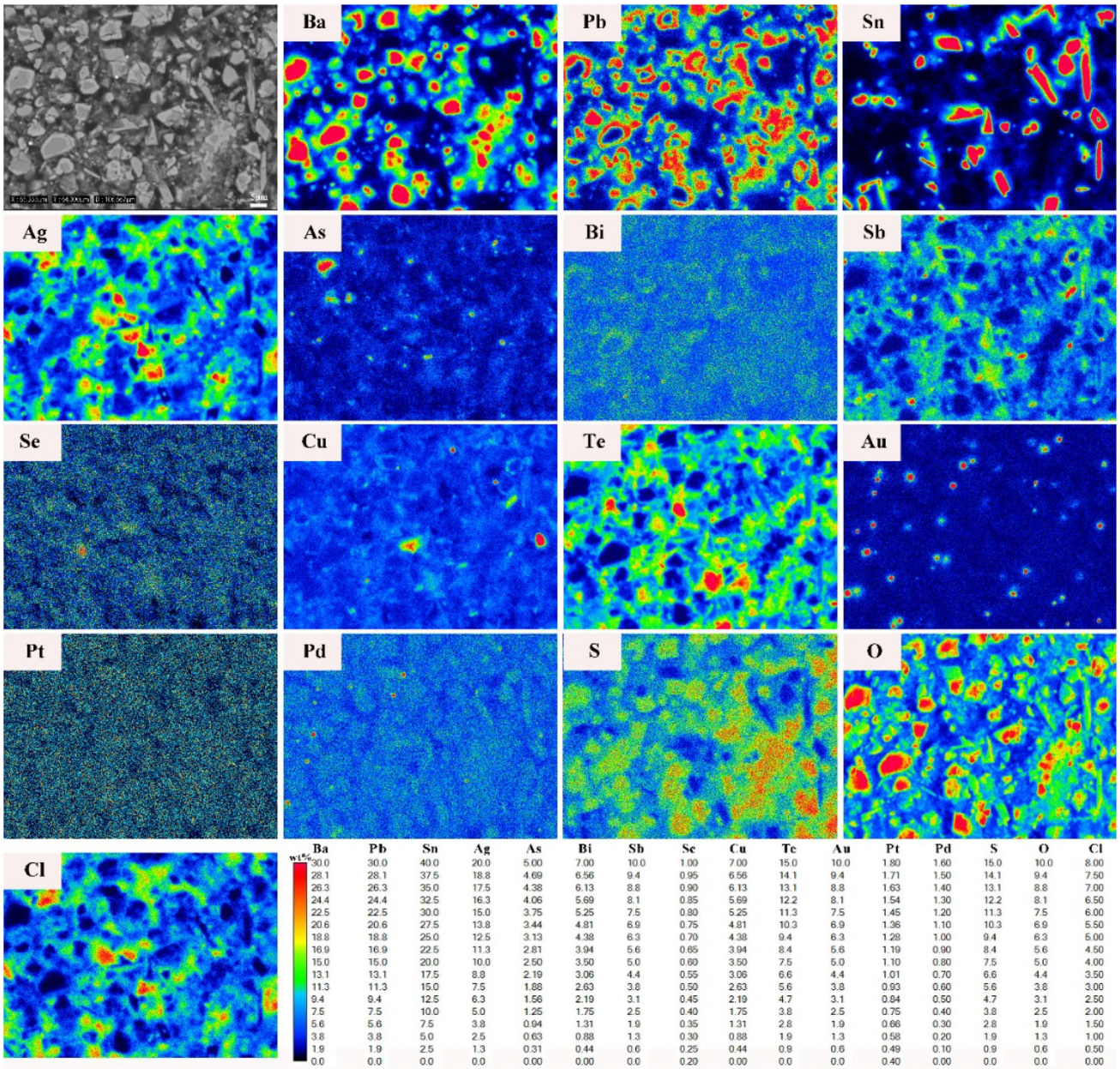

wt%	Ba	Pb	Sn	Ag	As	Bi	Sb	Se	Cu	Te	Au	Pt	Pd	S	O	Cl
30.0	30.0	30.0	40.0	20.0	5.00	7.00	10.0	1.00	7.00	15.0	10.0	1.80	1.60	15.0	10.0	8.00
28.1	28.1	28.1	37.5	18.8	4.69	6.56	9.4	0.95	6.56	14.1	9.4	1.71	1.50	14.1	9.4	7.50
26.3	26.3	26.3	35.0	17.5	4.38	6.13	8.8	0.90	6.13	13.1	8.8	1.63	1.40	13.1	8.8	7.00
24.4	24.4	24.4	32.5	16.3	4.06	5.69	8.1	0.85	5.69	12.2	8.1	1.54	1.30	12.2	8.1	6.50
22.5	22.5	22.5	30.0	15.0	3.75	5.25	7.5	0.80	5.25	11.3	7.5	1.45	1.20	11.3	7.5	6.00
20.6	20.6	20.6	27.5	13.8	3.44	4.81	6.9	0.75	4.81	10.3	6.9	1.36	1.10	10.3	6.9	5.50
18.8	18.8	18.8	25.0	12.5	3.13	4.38	6.3	0.70	4.38	9.4	6.3	1.28	1.00	9.4	6.3	5.00
16.9	16.9	16.9	22.5	11.3	2.81	3.94	5.6	0.65	3.94	8.4	5.6	1.19	0.90	8.4	5.6	4.50
15.0	15.0	15.0	20.0	10.0	2.50	3.50	5.0	0.60	3.50	7.5	5.0	1.10	0.80	7.5	5.0	4.00
13.1	13.1	13.1	17.5	8.8	2.19	3.06	4.4	0.55	3.06	6.6	4.4	1.01	0.70	6.6	4.4	3.50
11.3	11.3	11.3	15.0	7.5	1.88	2.63	3.8	0.50	2.63	5.6	3.8	0.93	0.60	5.6	3.8	3.00
9.4	9.4	9.4	12.5	6.3	1.56	2.19	3.1	0.45	2.19	4.7	3.1	0.84	0.50	4.7	3.1	2.50
7.5	7.5	7.5	10.0	5.0	1.25	1.75	2.5	0.40	1.75	3.8	2.5	0.75	0.40	3.8	2.5	2.00
5.6	5.6	5.6	7.5	3.8	0.94	1.31	1.9	0.35	1.31	2.8	1.9	0.66	0.30	2.8	1.9	1.50
3.8	3.8	3.8	5.0	2.5	0.63	0.88	1.3	0.30	0.88	1.9	1.3	0.58	0.20	1.9	1.3	1.00
1.9	1.9	1.9	2.5	1.3	0.31	0.44	0.6	0.25	0.44	0.9	0.6	0.49	0.10	0.9	0.6	0.50
0.0	0.0	0.0	0.0	0.0	0.00	0.00	0.0	0.20	0.00	0.0	0.0	0.40	0.00	0.0	0.0	0.00

Fig. 3 EPMA maps of the main metals in the decopperized anode slime

IRIS Intrepid II XSP). The leaching rate was calculated using the following formula:

$$\eta = \frac{\rho \cdot V}{m \cdot w \cdot 1000} \times 100\%$$

where η (%) represents the leaching rate; ρ (μg/mL) and m (g) are the concentration of various elements in the leaching solution and the quantity of the decopperized anode slime, respectively; and V (mL) and w (%) are the leaching solution volume and the content of the corresponding elements in the decopperized anode slime before leaching, respectively.

The phase composition of the main metals in the decopperized anode slime was determined using JXA 8200 EPMA with wavelength dispersion. When analyzing the element surface distribution, EPMA worked at an accelerating voltage of 20 kV and a probe current of 50 nA. When quantitatively analyzing the content of the elements, EPMA worked at an accelerating voltage of

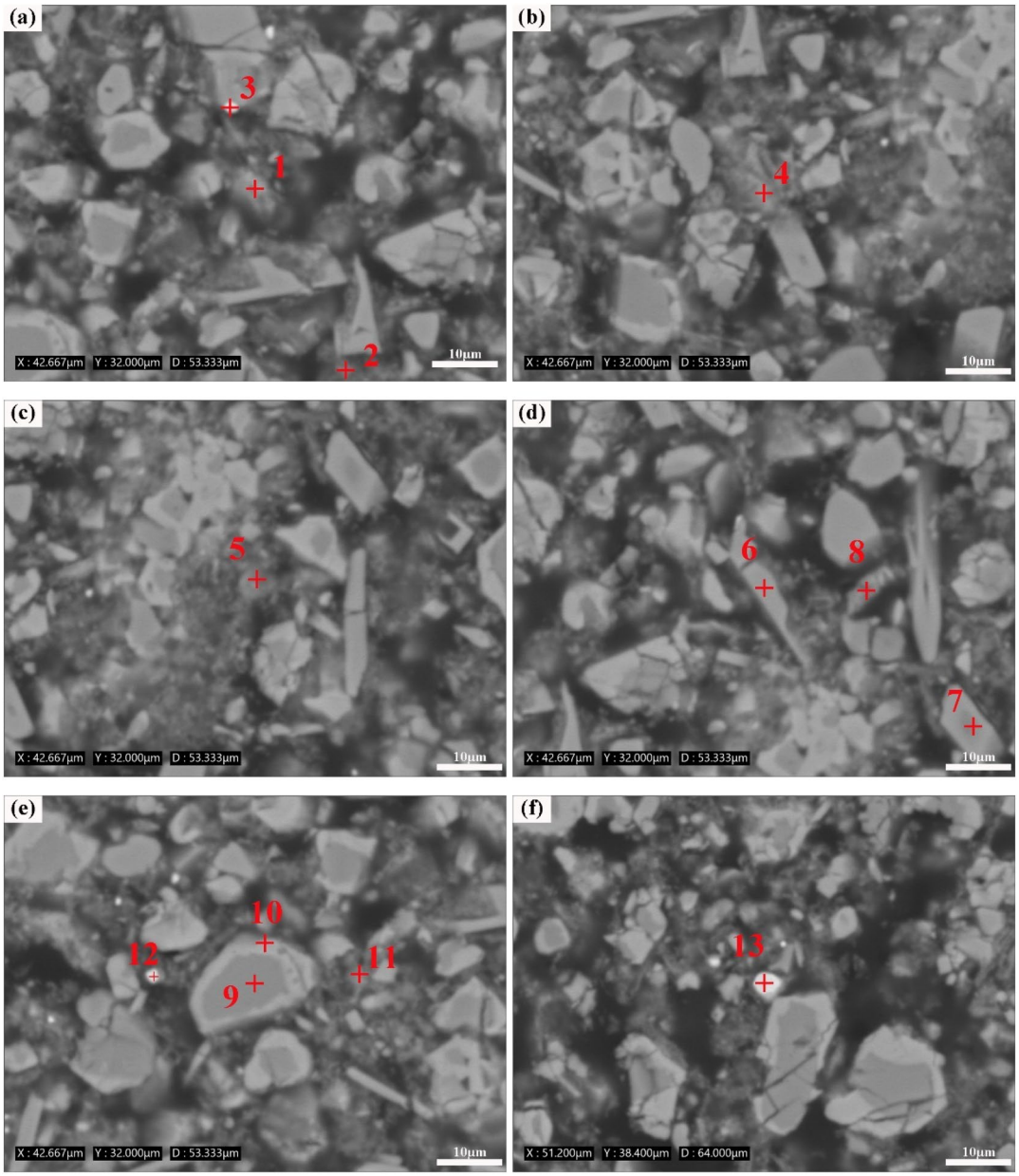

Fig. 4 BSE maps and analysis points for the decopperized anode slime, *X* and *Y* represent the horizontal position of the electron probe lens, and *D* represents the height of the lens

20 kV and a probe current of 10 nA. The ZAF correction procedure was applied. $BaSO_4$ was the standard for Ba, S, and O, while metallic substances were the standards for Pb, Sn, Ag, Sb, Se, Cu, Bi, Te, Au, Pt, and Pd. GeAs and $Na_4AlBeSi_4O_{12}Cl$ (Tugtupite) were used as the standard for As and Cl, respectively. X-ray fluorescence spectrometry (Philips PW2400) was used to determine the chemical composition of the leaching residue.

Result and Discussion

The Effect of Leaching Time

The curve of the leaching rate over time is shown in Fig. 6. The leaching efficiencies of Au, Pt, Pd, and Se reached equilibrium earlier due to differences in occurrence states.

Table 3 Element content for the selected points in Fig. 4 quantitatively determined by EPMA (at%)

Point	Ba	Pb	Ag	Sn	Te	Sb	Au	Cu	Se	As	Bi	Pt	Pd	O	S	Cl
1	1.236	0.989	27.314	1.265	14.321	0	0	1.134	0	1.021	0.082	0.002	0	41.669	6.760	4.207
2	0.352	0.136	19.417	5.802	5.017	0	0	1.602	0	0.898	0.143	0.053	0	50.045	2.630	13.905
3	5.531	4.810	1.921	0.191	0.671	0	36.957	0.191	0	0	0	0.146	1.594	36.099	11.100	0.789
4	0.224	0.159	19.482	2.227	11.407	0	0.013	1.893	0	1.191	0.330	0.024	0	50.673	3.651	8.727
5	4.656	3.505	6.021	1.152	4.137	0	0.037	0.762	0	0.570	0	0	0	64.879	8.668	5.616
6	0.071	0.068	0.298	28.311	0.661	0	0	0.051	0	0.026	0.028	0.009	0	70.048	0.193	0.236
7	0.213	0.089	0.127	22.475	1.620	0	0	34.466	0	0	0.021	0	0	40.801	0.111	0.078
8	0.914	0.868	13.462	1.692	5.359	7.491	0.169	6.220	0	1.047	0.133	0.143	0.026	51.225	5.128	6.124
9	21.378	0	1.595	0	0	0	0	0.024	0	0.034	0.054	0.009	0.002	57.081	19.778	0.041
10	11.334	9.523	3.955	0.055	0.230	0.086	0	0.420	0	0	0	0	0	54.988	18.932	0.476
11	1.570	1.290	15.317	16.731	6.509	0	0	1.872	0	0.976	0.019	0.075	0	43.528	4.866	7.246
12	1.840	1.719	7.848	0.493	2.064	0	52.072	0.121	1.606	0.563	0.242	0.027	0.983	17.847	5.643	6.932
13	0.513	0	1.558	0	0.031	0	86.261	0.401	2.437	0.0456	0.627	0	2.595	4.895	0.275	0.360

Table 4 The occurrence state and embedding characteristics of the main metal element in the decopperized anode slime

Element	Occurrence state	Embedding characteristics
Ba	$BaSO_4$, $(Ba_xPb_y)SO_4$	$BaSO_4$ was the core phase, and $(Ba_xPb_y)SO_4$ was the shell phase
Pb	$(Ba_xPb_y)SO_4$	Shell phase
Sb	Sb_2O_3	Coexisted with Ag-enrichment
Ag	AgCl, Ag_2Te, Ag_2SO_4, Ag_2O, Ag, Ag_2Se	Ag_2SO_4 was embedded in $(Ba_xPb_y)SO_4$
Se	SeO_2, Ag_2Se	Ag_2Se was embedded in the metallic phase
As	As_2O_3	Wrapped by Ag-enrichment
Bi	Bi_2O_3	Embedded in $(Ba_xPb_y)SO_4$
Cu	CuO, $CuSO_4$, Cu_2Te, Cu	CuO, Cu_2Te, and Cu were wrapped in $(Ba_xPb_y)SO_4$, SnO_2 particles, and the metallic phase, respectively
Te	Ag_2Te, TeO_2, Te, $AuTe_2$, Cu_2Te	Ag_2Te coexisted with Ag-enrichment. TeO_2 coexisted with SnO_2 particles. Te and $AuTe_2$ were embedded in the metallic phase
Au	Au, $AuTe_2$	Main components of the metallic phase
Pt	Pt, PtO_2	Mainly embedded in the metallic phase, and few coexisted with Ag-enrichment
Pd	Pd, PdO	Mainly embedded in the metallic phase, and few coexisted with Ag-enrichment

It can also be seen from Fig. 5 that the ΔG_r^{θ} of reactions (5) to (17) were relatively more negative. This indicates that the substances of the metallic phase will react preferentially. The leaching efficiencies of platinum and palladium remained stable at 80% and 90% with increasing reaction time, respectively, because PtO_2 and PdO were encapsulated by Ag-enrichment. In addition, the maximum leaching rate of Bi remained stable at approximately 57% with increasing leaching time. The reasons are as follows: Bi_2O_3 was encapsulated by $(Ba_xPb_y)SO_4$; Bi^{3+} can form an insoluble substance such as $Bi(OH)SO_4$ [23] in SO_4^{2-} medium, and the reaction is as follows:

$$Bi^{3+} + SO_4^{2-} + H_2O = Bi(OH)SO_4 + H^+ \quad (18)$$

With the extension of the leaching time, the leaching efficiencies of Cu, As, and Sb increased gently, whereas those of Sn, Pb, and Ag appeared unaffected. Comprehensively, the leaching time was selected to be 60 min.

The Effect of Liquid–Solid Ratio

As an integral factor in the leaching process, the importance of the liquid–solid ratio is undeniable. In this study, the leaching efficiencies of the main metals were observed in the liquid–solid ratio of 1 mL/g to 8 mL/g, and the results are shown in Fig. 7. Notably, after the solid–liquid separation process, it was found that there were still insoluble substances of AgCl and $PbSO_4$ in the filtrate, as shown in Fig. 8. Due to the ppm concentration of lead and silver ions in the solution and the high concentrations of SO_4^{2-} and Cl^-,

Table 5 Mineral phase composition of decopperized anode slime

Element	Phase	Content (wt%)
Cu	CuO	25.64
	CuS	3.59
	Cu	6.67
	$CuSO_4$	38.46
	Residue	25.64
	ΣCu	100.00
Ag	Ag	12.91
	Ag_2O	3.03
	Ag_2SO_4	13.36
	AgCl	11.67
	$Ag_2S + Ag_2Se$	55.60
	Ag in sulfide minerals	0.11
	Ag in iron manganese minerals	2.92
	Ag encapsulated in insoluble minerals	0.40
	ΣAg	100.00
Te	Ag_2Te	3.12
	CuTe	3.74
	$Te + AuTe_2$	93.14
	ΣTe	100.00

which formed extremely fine particles of lead sulfate and silver chloride. The leaching efficiencies of Se, Te, Cu, and Bi were less affected by the liquid–solid ratio when excessive leaching reagents were used. In comparison, with an increase in the liquid–solid ratio, the leaching efficiencies of Pb and Ag rose, while those of Au, Pt, and Pd decreased. The possible reasons are as follows: first, as the liquid content increased, the Pb and Ag phases came into fuller contact with the leaching reagent, generating AgCl and $PbSO_4$, which enhanced the encapsulation of Au, Pt, and Pd; second, the decrease in $NaClO_3$ concentration led to a decline in the leaching efficiencies of Au, Pt, and Pd. To exist stably in chlorinated solution, Au, Pt, and Pd need to be oxidized to high valence states of $AuCl_4^-$ [18, 24, 25], $PtCl_6^{2-}$ [18, 25], and $PdCl_4^{2-}$ [24], respectively. The reduction of the liquid–solid ratio can be favored for the subsequent enrichment of SPMs and wastewater treatment. Comprehensively, the liquid–solid ratio was selected to be 1 mL/g.

The Effect of H_2SO_4 Concentration

Figure 9 shows the effect of H_2SO_4 concentration on the leaching of Pb, Sn, Ag, Sb, Se, Cu, Bi, Te, Au, Pt, and Pd. It is worth noting that Ag will exist in the solution as $AgHSO_4$ [26] or $AgCl_{n+1}^{n-}$ [21] in the case of excessive H_2SO_4 and low acidity, which led to an increase in Ag leaching efficiency with the increase in H_2SO_4 concentration.

$$Ag_2SO_4 + H_2SO_4 = 2AgHSO_4 \tag{19}$$

$$AgCl + nCl^- = AgCl_{n+1}^{n-} \tag{20}$$

Interestingly, the leaching efficiencies of Cu and Se were 35.08% and 18.43%, respectively, at 0 mol/L H_2SO_4, confirming the presence of water-soluble phases such as $CuSO_4$ and SeO_2. The leaching efficiencies of Au, Pt, Pd,

Table 6 The possible reaction during the chlorination leaching of the decopperized anode slime

Number	Reaction
1	$CuO + 2H^+ = Cu^{2+} + H_2O$
(2)	$SeO_2 + H_2O = H_2SeO_3$
(3)	$TeO_2 + 4H^+ + 6Cl^- = TeCl_6^{2-} + 2H_2O$
(4)	$PdO + 2H^+ + 4Cl^- = PdCl_4^{2-} + H_2O$
(5)	$Ag + \frac{1}{6}ClO_3^- + H^+ + \frac{5}{6}Cl^- = AgCl\downarrow + 0.5H_2O$
(6)	$Au + 0.5ClO_3^- + 3H^+ + 3.5Cl^- = AuCl_4^- + 1.5H_2O$
(7)	$Pd + \frac{1}{3}ClO_3^- + \frac{11}{3}Cl^- + 2H^+ = PdCl_4^{2-} + H_2O$
(8)	$Ag_2O + 2H^+ + 2Cl^- = 2AgCl\downarrow + H_2O$
(9)	$Te + \frac{2}{3}ClO_3^- + \frac{16}{3}Cl^- + 4H^+ = TeCl_6^{2-} + 2H_2O$
(10)	$Pt + \frac{2}{3}ClO_3^- + \frac{16}{3}Cl^- + 4H^+ = PtCl_6^{2-} + 2H_2O$
(11)	$PtO_2 + 6Cl^- + 4H^+ = PtCl_6^{2-} + 2H_2O$
(12)	$Cu + 2H^+ + \frac{1}{3}ClO_3^- = Cu^{2+} + \frac{1}{3}Cl^- + H_2O$
(13)	$Ag_2Se + ClO_3^- + 2H^+ + Cl^- = 2AgCl\downarrow + H_2SeO_3$
(14)	$Sn + \frac{2}{3}ClO_3^- = SnO_2\downarrow + \frac{2}{3}Cl^-$
(15)	$Ag_2Te + ClO_3^- + 6H^+ + 7Cl^- = 2AgCl\downarrow + TeCl_6^{2-} + 3H_2O$
(16)	$Cu_2Te + \frac{4}{3}ClO_3^- + \frac{14}{3}Cl^- + 8H^+ = 2Cu^{2+} + TeCl_6^{2-} + 4H_2O$
(17)	$AuTe_2 + \frac{11}{6}ClO_3^- + 11H^+ + \frac{85}{6}Cl^- = AuCl_4^- + 2TeCl_6^{2-} + 5.5H_2O$

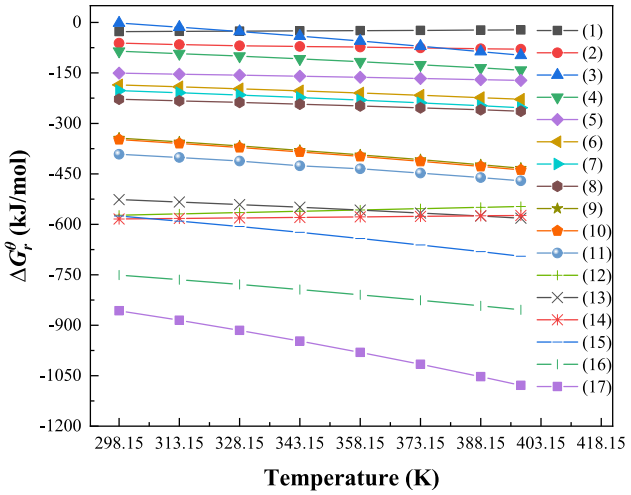

Fig. 5 The Gibbs free energy variation curve of the possible reaction during the chlorination leaching process of the decopperized anode slime with temperature

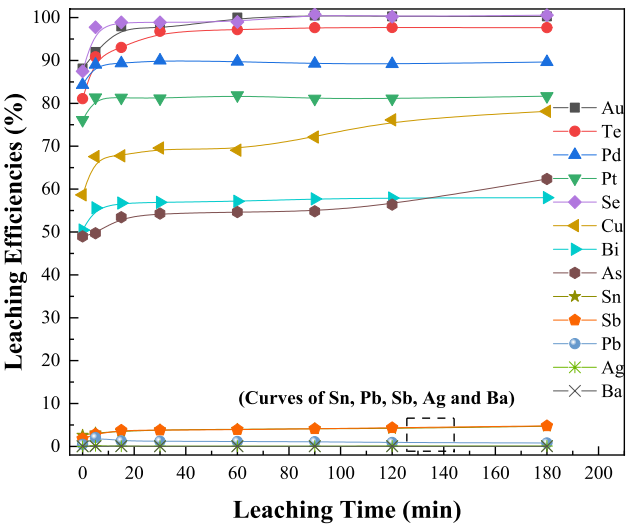

Fig. 6 Effect of leaching time on the leaching rate of each element (T = 80 °C , L/S = 4 mL/g, H_2SO_4 = 3 mol/L, NaCl = 100 g/L, $NaClO_3$ = 0.2 g)

Te, and Se significantly increased with the increase of H_2SO_4 concentration, and all tended to be stable after the H_2SO_4 concentration was ≥ 1 mol/L. When the concentration of H_2SO_4 concentration increased from 1 mol/L to 2 mol/L, the leaching efficiencies of As, Sb, and Bi increased from 18.22%, 0.93%, and 51.19% to 41.83%, 1.61%, and 56.31% respectively. Both As, Sb, and Bi are the main impurities in high-purity tellurium [17]. Comprehensively, the H_2SO_4 concentration was chosen to be 1 moL/L.

The Effect of NaCl Concentration

The leaching behaviors of Pb, Sn, Ag, Sb, Se, Cu, Bi, Te, Au, Pt, and Pd were studied in the NaCl concentration range of 0–200 g/L, as shown in Fig. 10. When the NaCl concentration increased from 0 g/L to 100 g/L, the leaching efficiencies of Te, Au, Pt, and Pd increased significantly, from 27.41 to 93.80%, from 0.29 to 99.10%, from 7.84 to 95.11% and from 4.39 to 99.62%, respectively. The cause of this phenomenon is that Te, Au, Pt, and Pd can complex chloride ions to form multi-coordination compounds in an acidic system. When the NaCl concentration increased from 60 g/L to 80 g/L, Bi leaching efficiency enhanced obviously. It can be explained that Bi_2O_3 was soluble in hydrochloric acid [27, 28], and may reacted by following the formula in the H_2SO_4 + NaCl system,

$$Bi_2O_3 + H_2SO_4 + NaCl = 2BiCl_3 + 3Na_2SO_4 + 3H_2O \quad (21)$$

In addition, when the NaCl concentration exceeded 30 g/L, the leaching efficiency of as was stable at 27% around. The reason is that the leaching of As was affected by the concentration of H^+, as shown in Fig. 9. Comprehensively, the NaCl concentration was chosen to be 100 g/L.

The Effect of the Dosage of $NaClO_3$

The reagent consumption is a statistical index in the production process. After calculation, the theoretical dosage of $NaClO_3$ required for 5 g of the decopperized anode is 0.12 g. This section discussed the influence of 0 to 1.75 times the theoretical dosage, as shown in Fig. 11. Without adding $NaClO_3$, the leaching efficiencies of Te, Se, Pt, and Pd were 42.51%, 60.85%, 20.34%, and 7.44% respectively. This indicates that some Te, Se, Pt, and Pd existed in the form of oxides. These oxides formed multi-coordination compounds with chloride ions, which dissolved in the leachate under acidic conditions and Se presented in the solution as H_2SeO_3. As the dosage of $NaClO_3$ increased, the leaching of Te, Se, Au, Pt, and Pd was promoted, while that of Cu was affected imperceptibly. By contrast, with the increase in $NaClO_3$ dosage, the Bi leaching efficiency increased from 42.43 to 48.40% and then decreased to 44.12%. In addition, the As leaching efficiency decreased with the increase in oxidant dosage. The reasons for the phenomena of As and Bi are as follows: as was oxidized to a high valence state, such as AsO_4^{3-}, which is difficult to dissolve in the sulfuric acid system [29]; moreover, Bi^{3+} combined with AsO_4^{3-} to insoluble substances such as $BiAsO_4$ [30, 31], and the reactions involved are as follows:

$$Bi^{3+} + AsO_4^{3-} = BiAsO_4 \quad (22)$$

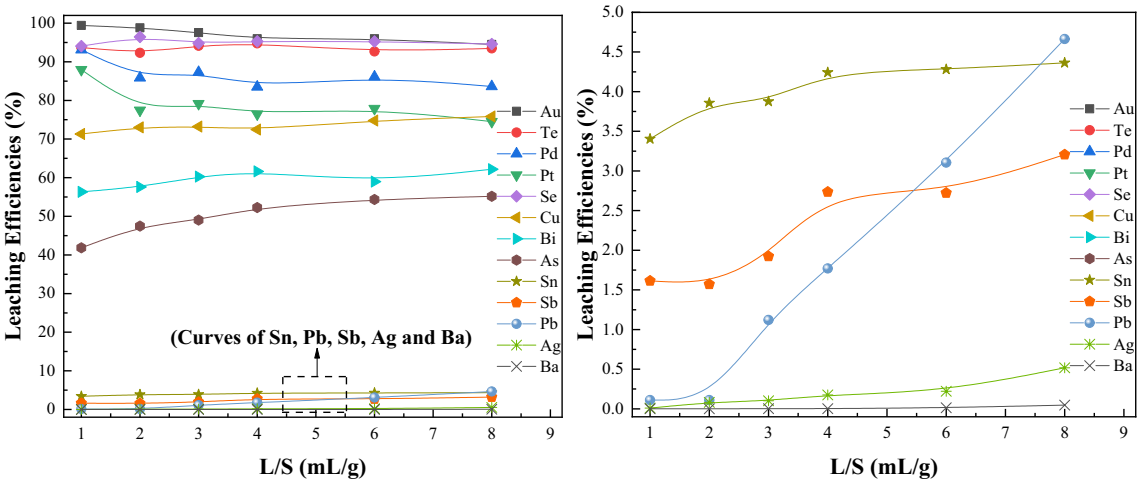

Fig. 7 Effect of L/S on the leaching rate of each element (T = 80 °C , Time = 60 min, H_2SO_4 = 3 mol/L, NaCl = 100 g/L, $NaClO_3$ = 0.2 g)

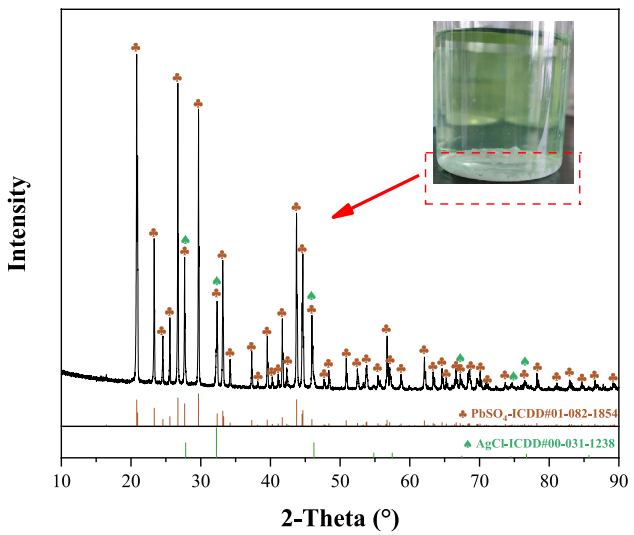

Fig. 8 The XRD pattern of insoluble substances in leaching solution

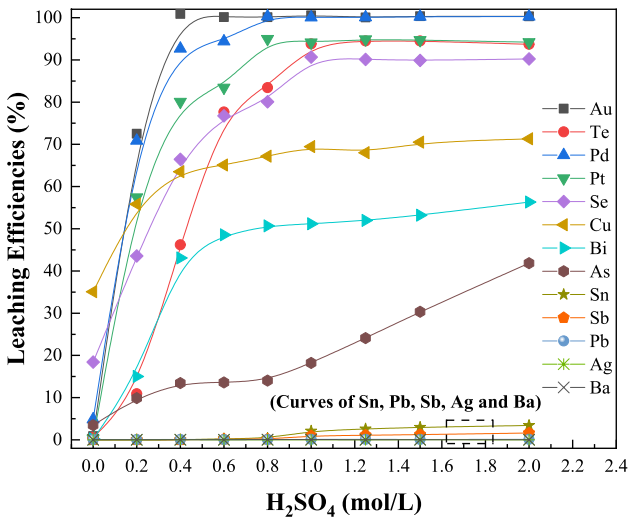

Fig. 9 Effect of sulfuric acid concentration on the leaching rate of each element (T = 80 °C , Time = 60 min, NaCl = 100 g/L, L/S = 1 mL/g, $NaClO_3$ = 0.2 g)

Comprehensively, the multiple of the theoretical dosage of $NaClO_3$ was chosen to be 1.25 times, which is the 3% by mass of the decopperized anode slime.

The Effect of Leaching Temperature

The reaction temperature is an important technical parameter in the production process, and its impact on the leaching process is shown in Fig. 12. When the temperature increased from 5 °C to 80 °C, the leaching efficiencies of Au, Te, Pt, Pd, and Se increased from 0.12%, 32.68%, 20.34%, 2.09%, and 54.66% to 100.79%, 97.69%, 94.47%, 100.38%, and 81.67%, respectively. High temperatures can promote the diffusion between ions and reduce the activation energy required for the reaction [3]. However, Cl^- volatilized in the form of chlorine, and the concentration of Cl^- decreased, which led to a slight decrease in the leaching rate of Te, Au, Pt, and Pd. Interestingly, the leaching efficiency of as declined most significantly. Therefore, the phase composition of leaching residue with the reaction temperature of 95 °C was analyzed. This result shows that As in the residue was mainly present in $PbBi_6O_4(AsO_4)_4$. This indicates that high temperature was conducive to the oxidation of as into a high valence state of AsO_4^{3-}, as shown in Fig. 13. Comprehensively, 80℃ was the appropriate leaching temperature.

The main elements content of leaching residue is shown in Table 7. The leaching residue contained 15.55% Ba, 14.79% Pb, 8.37% Ag, 8.52% Sn, 2.01% Sb, 1.23% Cu, and 0.26% Te, without Au. The leaching residue mainly contains

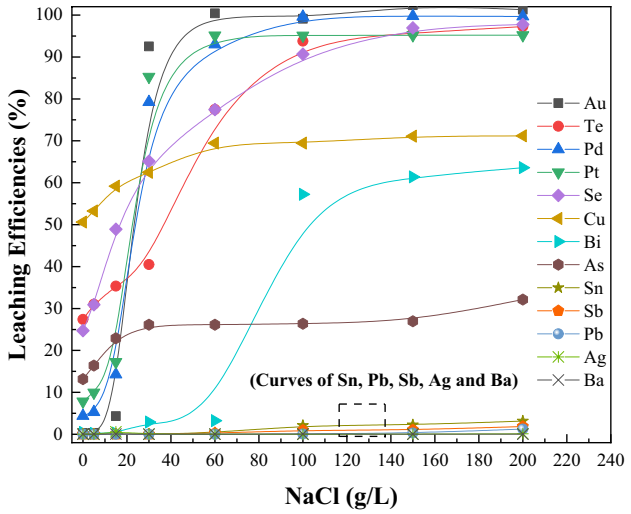

Fig. 10 Effect of NaCl concentration on the leaching rate of each element (T = 80 °C , time = 60 min, H_2SO_4 = 1 mol/L, L/S = 1 mL/g, $NaClO_3$ = 0.2 g)

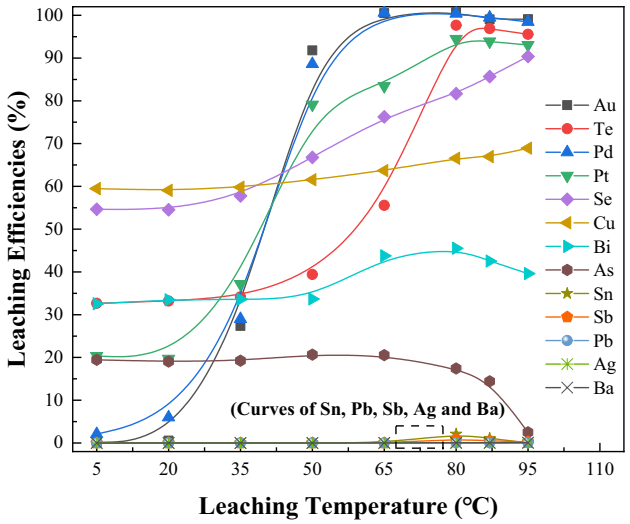

Fig. 12 Effect of the leaching temperature on the leaching rate of each element (Time = 60 min, H_2SO_4 = 1 mol/L, L/S = 1 mL/g, NaCl = 100 g/L, $NaClO_3$ = 0.15 g)

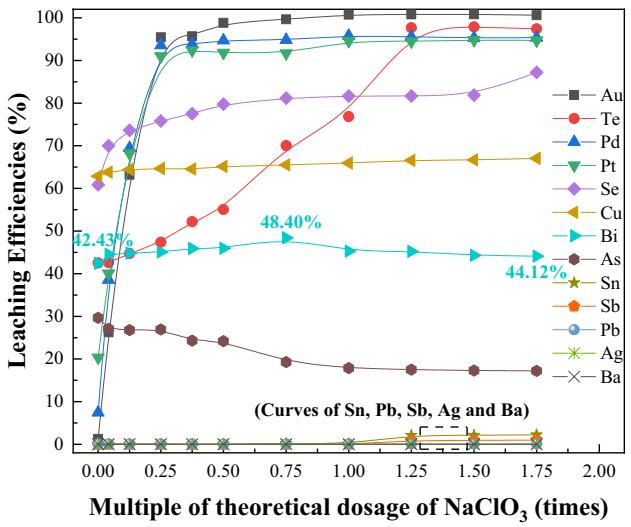

Fig. 11 Effect of the usage of $NaClO_3$ on the leaching rate of each element (T = 80℃, time = 60 min, H_2SO_4 = 1 mol/L, L/S = 1 mL/g, NaCl = 100 g/L)

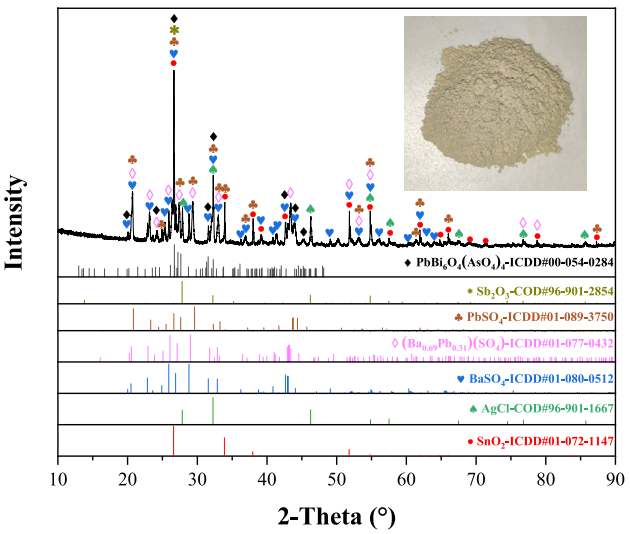

Fig. 13 The XRD pattern of the leaching residue at Temperature = 95 °C

phases such as SnO_2, $BaSO_4$, $(Ba_{0.69}Pb_{0.31})SO_4$, AgCl, $PbSO_4$, Sb_2O_3 and $PbBi_6O_4(AsO_4)_4$, as shown in Fig. 13.

In summary, the optimal reaction conditions for chlorination leaching of the decopperized anode slime were a reaction time of 60 min, H_2SO_4 concentration of 1 mol/L, L/S = 1 mL/g, NaCl concentration of 100 g/L, and $NaClO_3$ addition of 3% by the mass of the decopperized anode slime. The leaching efficiencies of Pb, Sn, Ag, Sb, Se, Cu, Bi, Te, Au, Pt, and Pd under this condition were 0.07%, 2.10%, 0.00%, 0.89%, 81.67%, 66.56%, 45.52%, 97.69%, 100.79%, 94.47%, 100.38%, respectively.

Conclusions

Effects of leaching time, liquid-solid ratio, H_2SO_4 concentration, the dosage of $NaClO_3$, and leaching temperature on the leaching behavior of the main elements were experimentally investigated. In the H_2SO_4+NaCl system, increasing the H_2SO_4 concentration, NaCl concentration, or temperature can promote the leaching of Te, Au, Pt, and Pd. Addicting $NaClO_3$ scarcely affected the leaching of Se, Cu, and Bi while impacting that of Te, Au, Pt, and Pd. The leaching efficiencies of Te, Au, Pt, and Pd reached

Table 7 Main chemical components of the leaching residue at Temperature = 95 °C

Element	Ba	Pb	Ag	Sn	Sb	Cu	Te
Content (wt%)	15.55	14.79	8.37	8.52	2.01	1.23	0.26
Element	As	Bi	Si	O	S	Cl	
Content (wt%)	0.79	0.23	1.23	28.58	6.05	3.87	

97.69%, 100.79%, 94.47%, and 100.38%, respectively. The possible reasons were discussed to explain the leaching differences between the SPMs and base metals. The SPMs and base metals can be separated by one-step chlorination oxidation leaching. This process provides an efficient and short technology for industrial production.

Acknowledgements This work was supported by the National Key Research and Development Program of China (No. 2023YFC2907902) and the National Natural Science Foundation of China (No. U1802251).

Funding This article is funded by Key Technologies Research and Development Program, 2023YFC2907902, Chunfa Liao, National Natural Science Foundation of China, U1802251, Chunfa Liao.

Data availability The datasets used and/or analyzed are available from the corresponding author upon reasonable request.

References

1. International Copper Study Group (ICSG), The World Copper Factbook 2023, https://icsg.org/copper-factbook. Accessed 4 Jan 2024
2. S. Liu, Y. Cai, Y. Zhang, Z. Su, T. Jiang, Sep. Purif. Technol. **296** (2022). https://doi.org/10.1016/j.seppur.2022.121378
3. B. Li, J. Deng, W. Jiang, G. Zha, B. Yang, Sep. Purif. Technol. **310** (2023). https://doi.org/10.1016/j.seppur.2022.123059
4. J.-C. Lee, K. Kurniawan, K.W. Chung, S. Kim, Met. Mater. Int. **27**, 2160–2187 (2020). https://doi.org/10.1007/s12540-020-00716-7
5. Z. Dong, T. Jiang, B. Xu, J. Wu, Q. Li, Y. Yang, Sep. Purif. Technol. **328** (2024). https://doi.org/10.1016/j.seppur.2023.125053
6. B. Xu, J. Wu, Z. Dong, T. Jiang, Q. Li, Y. Yang, Appl. Surf. Sci. **551** (2021). https://doi.org/10.1016/j.apsusc.2021.149420
7. H. Luo, W.-Y. Wang, X. Yu, X.-J. Lei, L. Liu, G.-Z. Zha, W.-L. Jiang, B. Yang, B.-Q. Xu, Vacuum. **219** (2024). https://doi.org/10.1016/j.vacuum.2023.112737
8. I. Hadar, T.B. Song, W. Ke, M.G. Kanatzidis, Adv. Energy Mater. **9** (2019). https://doi.org/10.1002/aenm.201802766
9. W. Yang, X. Lan, Q. Wang, P. Dong, G. Wang, Front. Chem. **9** (2021). https://doi.org/10.3389/fchem.2021.593888
10. Y. Zeng, C. Liao, F. Liu, X. Zhou, ACS Omega. **8**, 10022–10029 (2023). https://doi.org/10.1021/acsomega.2c07251
11. G. Liu, Y. Wu, A. Tang, D.A. Pan, B. Li, Hydrometallurgy. **197** (2020). https://doi.org/10.1016/j.hydromet.2020.105460
12. M. Khanlarian, F. Rashchi, M. Saba, J. Environ. Manage. **235** 303–309 (2019). https://doi.org/10.1016/j.jenvman.2019.01.079
13. Z. Dong, T. Jiang, B. Xu, J. Yang, Y. Chen, Q. Li, Y. Yang, Chem. Eng. J. **393** (2020). https://doi.org/10.1016/j.cej.2020.124762
14. S. Rao, D. Wang, H. Cao, W. Zhu, L. Duan, Z. Liu, Sep. Purif. Technol. **300** (2022). https://doi.org/10.1016/j.seppur.2022.121696
15. L. Shao, J. Diao, C. Ji, G. Li, Hydrometallurgy. **191** (2020). https://doi.org/10.1016/j.hydromet.2019.105205
16. D.J. Lane, N.J. Cook, S.R. Grano, K. Ehrig, Miner. Eng. **98**, 110–121 (2016). https://doi.org/10.1016/j.mineng.2016.08.006
17. C.K. Sarangi, A.R. Sheik, B. Marandi, V. Ponnam, M.K. Ghosh, K. Sanjay, M. Minakshi, T. Subbaiah, Sustainability. **15** (2023). https://doi.org/10.3390/su151511919
18. S. Wang, L. Li, S.D. Wang, H. Wang, G.D. Wu, J. Mining Metall. Sect. B: Metall. **56**, 193–202 (2020). https://doi.org/10.2298/jmmb190915015w
19. Y. Zeng, J. Zou, C. Liao, F. Liu, X. Zhou, Miner. Eng. **168** (2022). https://doi.org/10.1016/j.mineng.2022.107749
20. C.W. Bale, E. Bélisle, P. Chartrand, S.A. Decterov, G. Eriksson, A.E. Gheribi, K. Hack, I.H. Jung, Y.B. Kang, J. Melançon, A.D. Pelton, S. Petersen, C. Robelin, J. Sangster, P. Spencer, M.A. Van Ende, Calphad **54**, 35–53 (2016). https://doi.org/10.1016/j.calphad.2016.05.002
21. A.J. Bard, R. Parsons, J. Jordan, *Standard potentials in aqueous solution* (Routledge, Milton Park, 2017).
22. M. Pourbaix, *Atlas of Electrochemical Equilibria in Aqueous Solutions* (National Association of corrosion Engineers, Houston, 1974).
23. T. Dai-Di, J. Chao-Jin, Y. Yue-Xin, D. Tao, Mining and Metallurgical Engineering. **36**, 100–103 (2016).
24. B. Jind, M.F. Jiménez-Moreno, G. Chauhan, A. Aguirre-Soto, G.F. Payne, S.O. Martínez-Chapa, Adv. Mater. Interfaces. **11** (2023). https://doi.org/10.1002/admi.202300543
25. G. Martinez-Ballesteros, J.L. Valenzuela-García, A. Gómez-Alvarez, M.A. Encinas-Romero, F.A. Mejía-Zamudio, A.D.J. Rosas-Durazo, R. Valenzuela-Frisby, Recycling. **6** (2021). https://doi.org/10.3390/recycling6040067
26. L. Weifeng, L. Younian, Y. Tianzu, C. Lin, Z. Duchao, W. An, J. Central South Univ. Sci. Technol. **44**, 2192–2199 (2013).
27. P. Ketwong, M. Takashima, A. Nitta, P. Pookmanee, B. Ohtani, J. Environ. Chem. Eng. **6**, 2048–2054 (2018). https://doi.org/10.1016/j.jece.2018.01.062
28. A.P. Reverberi, P.S. Varbanov, S. Lauciello, M. Salerno, B. Fabiano, J. Clean. Prod. **198**, 37–45 (2018). https://doi.org/10.1016/j.jclepro.2018.07.011
29. R. Hosokawa, H. Okawa, Japn J. Appl. Phys. **51** (2012). https://doi.org/10.1143/jjap.51.07gd14
30. N.J. Cook, K. Ehrig, C.L. Ciobanu, S.A. King, V. Liebezeit, A.D. Slattery, Miner. Eng. **206** (2024). https://doi.org/10.1016/j.mineng.2023.108539
31. J.G. Speight, *Langes Handbook of Chemistry* (McGraw-Hill Education, New York, 2004).